Composite Structures 234 (2020) 111664

Contents lists available at ScienceDirect

Composite Structures

journal homepage: www.elsevier.com/locate/compstruct

Deformation analysis of fibre-reinforced polymer reinforced concrete beams by tension-stiffening approach

P.L. Ng[a,b,*], J.A.O. Barros[c], G. Kaklauskas[d], J.Y.K. Lam[e]

[a] Department of Civil Engineering, The University of Hong Kong, Hong Kong, China
[b] Faculty of Civil Engineering, Vilnius Gediminas Technical University, Vilnius, Lithuania
[c] ISISE and IB-S, University of Minho, Guimarães, Portugal
[d] Institute of Building and Bridge Structures, Vilnius Gediminas Technical University, Vilnius, Lithuania
[e] AECOM, Hong Kong, China

ARTICLE INFO

Keywords:
Deflection
Fibre-reinforced polymer
Finite element method
FRP reinforcement
Member analysis
Serviceability
Tensile stress block
Tension-stiffening

ABSTRACT

Fibre-reinforced polymer (FRP) is free from corrosion problem and is a viable alternative reinforcement material for concrete structures in lieu of steel reinforcing bars. Since FRP has lower elastic modulus compared to steel, the serviceability aspect of FRP reinforced concrete (FRP-RC) members should be particularly considered in the structural analysis and design. This study addresses the deformation analysis of FRP-RC flexural members with thorough consideration of the tension-stiffening phenomenon in post-cracking state. The approaches for analyzing the tension-stiffening flexural response of FRP-RC beams are presented. These include the use of empirical or theoretical models to compute effective flexural stiffness, the use of finite element method in conjunction with nonlinear constitutive material models, and the use of tensile stress block in combination with member analysis. Among them, the latter is a relatively simple analysis approach. Aiming for serviceability assessment of FRP-RC beams in structural engineering practice to circumvent sophisticated theoretical approaches and constitutive models, parametrized tensile stress block is derived based on tension stress fields computed from finite element analysis, and is proposed for use in member analysis for prediction of deflections. Four FRP-RC beam specimens tested in the literature are analyzed to verify the proposed tensile stress block. Close agreement between the experimental and analytical results is achieved, thereby endorsing the applicability and reliability of the proposed method.

1. Introduction

The use of steel as reinforcement material in reinforced concrete (RC) structures is widespread in the construction industry, however, the steel corrosion problem is a major factor impairing the durability of RC structures, and it invokes costly repair and maintenance works. The structural effects of corrosion of steel bars are two-folded. Firstly, the effective area of reinforcement for resisting load will decrease. Secondly, as the corrosion product is more voluminous than un-corroded steel, the volume expansion will induce bursting stresses in concrete that leads to cracking, which would allow ingress of moisture and chemicals, by further accelerating the corrosion. Being corrosion-free, the use of fibre-reinforced polymer (FRP) reinforcing bars is a viable alternative reinforcement material option in structural design and applications [35,83]. Apart from their chemically inert characteristics, FRP has additional advantages over conventional steel reinforcement, including high tensile strength, high strength-to-weight ratio, magnetic neutrality, and ease of handling. Moreover, with the increasing popularity of utilising FRP in construction that leads to drop in material cost, in tandem with the surging of price of steel, the cost premium of FRP relative to steel is narrowing down and vanishing. This offers further commercial initiatives of using FRP reinforcement. On the other hand, there are disadvantages of FRP reinforcement, including relatively low modulus of elasticity and low ductility that may adversely affect the structural performance, especially in the aspect of serviceability to which attention should be paid [39].

From practical engineering design viewpoint, though the design methodology of FRP reinforced concrete (FRP-RC) beams has been established and incorporated in dedicated design manuals and standards such as *fib* (Fédération international du béton) Bulletin 40 [28] and American Concrete Institute ACI 440.1R-15 (ACI-440) [3], the design philosophy is largely based on ultimate strength capacities while further research is still needed for the serviceability issues. The deformation analysis and deflection calculation of FRP-RC beams are relatively

* Corresponding author.
E-mail address: irdngpl@gmail.com (P.L. Ng).

https://doi.org/10.1016/j.compstruct.2019.111664
Received 4 April 2019; Accepted 3 November 2019
Available online 06 November 2019

complicated and these present challenges to structural engineers. It is understood that upon cracking of a RC member, the tension force is entirely resisted by the reinforcement at the cracked sections. Nevertheless, the intact concrete between adjacent cracks is still able to carry certain level of tensile stresses and contribute to the stiffness of concrete member. Such tension-stiffening phenomenon has been widely investigated in conventional steel RC flexural members [20,40,79,64,62]. In contrast with steel reinforcement, common FRP reinforcement typically produced with glass fibre has remarkably lower modulus of elasticity [42], meaning that at the same tensile stress level, the elongation of FRP reinforcement is much greater than that of steel reinforcement. Moreover, the bond stiffness and bond strength between FRP reinforcement and concrete are considerably lower than those between steel reinforcement and concrete [4,6]. Therefore, FRP reinforcement is expected to exhibit larger elongations at cracked sections. This implies that larger deformations and curvatures would be sustained by the FRP-RC member. It has been reported in the literature that FRP-RC beams exhibited lower flexural stiffness compared to steel RC beams [63].

For the purpose of accounting for the tension-stiffening effect in RC members, sophisticated constitutive material models can be integrated into finite element analysis, which is versatile and able to account for the variable nonlinear response of cracked structural members. Various models had been put forward to simulate the mechanical behaviour of concrete under multi-axial stress states [29,37], stress-crack width relation taking into account the fracture energy dissipation of crack initiation and propagation [19,1], and bond stress-slip relation taking into account the stress-transfer along the development length of reinforcement [27,18]. Albeit the high accuracy achievable by these models, they might not be suitable for day-to-day structural design works due to the large number of parameters required, whose valuation may require dedicated and specialized laboratory testing and is not straightforward. Moreover, the finite element method requires substantial manual effort for pre- and post-processing including establishing the numerical model and interpreting the numerical results. Apart from finite element analysis using sophisticated models, there are mainly two fundamental and practical approaches as described in the following. The first approach employs empirical or theoretical models to determine the effective flexural stiffness, which accounts for the reduction in stiffness of beam due to concrete cracking. The second approach incorporates the tensile stress block, which represents the integral tensile deformational characteristics of cracked RC, into member analysis. Compared to finite element method, member analysis is a relatively simple approach, and is particularly suitable for structural engineering practice.

Under the first approach, the flexural stiffness reduction due to cracking of RC beams can be reflected either by empirical or semi-empirical equations of effective moment of inertia, or by close-form tension-stiffening models or moment-curvature relationships such that the bond slip of reinforcement can be explicitly accounted for. Branson [16,17] proposed empirical equation of effective moment of inertia for the prediction of moment-curvature and load-deflection responses. The equation for effective moment of inertia stipulated in American Concrete Institute design code ACI 318M-14 [2] has been based on Branson's equation. While this approach is able to yield reasonable prediction of deflections in steel RC beams, its applicability to FRP-RC beams has to be confirmed by research. Experimental results of FRP-RC beams revealed that Branson's equation would underestimate beam deflections after cracking [82,13]. To extend the scope of applications of Branson's equation, a number of researchers [11,56,32,12,14,15] had introduced various parameters to modify Branson's equation to fit with the experimental results. However, previous attempts to modify Branson's equation had focused on fitting with respective sets of experimental results in particular, and a more universally applicable equation of effective moment of inertia of FRP-RC beams has been in lack. To formulate design guideline for FRP-RC beams, a modified version of Branson's equation has been recommended by ACI-440 [3].

In employing the effective moment of inertia, perfect bond is assumed with respect to the kinematic compatibility between concrete and reinforcement in any cross-section. Therefore, bond slip is either neglected or indirectly considered through adjusting the constitutive stress-strain relationships in the analysis [45]. To explicitly account for the bond slip of reinforcing bars along cracked sections, close-form tension-stiffening model and moment-curvature relationships have been derived by various researchers by taking into account various idealized bond stress-slip laws. For example, Marti et al. [55] assumed piece-wise constant bond stress-slip law and derived the tension chord model for both direct tension and flexural members. Kwak and Kim [44] assumed constant bond stiffness and incorporated empirical expression of plastic hinge length to derive a moment-curvature relation for RC flexural members. Castel et al. [21] assumed plastic bond behaviour and derived the effective tension active cross-section of RC beams. The research results for conventional steel RC members provided a basis for further extension to FRP-RC members.

Under the second approach, the tensile stress block is incorporated into member analysis. The tensile stress block for RC beams reflects the mechanical property of *reinforced* concrete in flexural tension zone (the tensile stress block is not a material model of plain concrete) for accounting the tension-stiffening effect [46]. Different tensile stress blocks have been devised for steel RC beams in the literature, for example, Schnobrich [74], Carreira and Chu [20], Beeby et al. [10], and Ng et al. [64]. However, research of the tension-stiffening phenomenon of FRP-RC beams is still limited in the sense that tensile stress block for deflection calculation of FRP-RC beams has not been recommended in any prevailing design code or standard. It is noteworthy to remark that Nayal and Rasheed [63] postulated a tensile stress block from adapting the multi-linear tensile stress block developed by Gilbert and Warner [33] for concrete slabs reinforced with steel bars, further research is nevertheless needed to define the geometry of the descending branch after first cracking.

From practical viewpoint, member analysis with the use of an appropriate tensile stress block is suggested for serviceability assessment [50,51] to circumvent the use of sophisticated theoretical models and constitutive models yet to achieve reasonably high accuracy. The present study examines the stresses and deformations of FRP-RC beams in the pre-cracking and post-cracking regime, with the aim to develop parametrized tensile stress block for analyzing the serviceability of FRP-RC beams. To verify the proposed tensile stress block, four FRP-RC beam specimens tested in the literature are analyzed. The numerical results are found to be in good agreement with the experimental results, thereby endorsing the applicability of the tensile stress block. Through this research, the use of the proposed tensile stress block for FRP-RC beams in conjunction with member analysis is validated and is advocated to the structural design practice.

2. Effective flexural stiffness

2.1. Empirical or semi-empirical effective moment of inertia

The effective moment of inertia recommended in ACI Committee 318 [2] is based on the semi-empirical equation proposed by Branson [16] for evaluating the deflection of cracked RC beams. The ACI-318 equation is given by:

$$I_e = \left(\frac{M_{cr}}{M_a}\right)^3 I_g + \left[1 - \left(\frac{M_{cr}}{M_a}\right)^3\right] I_{cr} \leqslant I_g \tag{1}$$

where I_e is the effective moment of inertia, I_g is the transformed gross section moment of inertia, I_{cr} is the transformed cracked moment of inertia, M_{cr} is the cracking moment and M_a is the maximum bending moment applied to the beam.

Subsequently, Benmokrane et al. [11] introduced two empirical reduction factors λ_1 and λ_2 to Branson's equation in order to correlate

with their experimental results of FRP-RC beams. The modified equation is expressed as:

$$I_e = \left(\frac{M_{cr}}{M_a}\right)^3 \frac{I_g}{\lambda_1} + \left[1 - \left(\frac{M_{cr}}{M_a}\right)^3\right] \lambda_2 I_{cr} \leqslant I_g \tag{2}$$

In Eq. (2), λ_1 and λ_2 were determined to be 7.0 and 0.84, respectively. The experimental investigation carried out by Al-Sunna et al. [5] showed that the reduction factor λ_1 is dependent on the reinforcement ratio and could be expressed as an exponential function of the reinforcement ratio and the modulus of elasticity of FRP.

Gao et al. [32] further modified Eq. (2) with another reduction factor to improve its agreement with additional experimental results in the literature. The modified equation is given by:

$$I_e = \left(\frac{M_{cr}}{M_a}\right)^3 \psi_d I_g + \left[1 - \left(\frac{M_{cr}}{M_a}\right)^3\right] I_{cr} \leqslant I_g \tag{3}$$

where

$$\psi_d = \psi_b \left(\frac{E_f}{E_s} + 1\right) \tag{4}$$

The reduction factor ψ_d is to account for the differences in the moduli of elasticity and bond characteristics between FRP and steel reinforcement. In Eq. (4), ψ_b is a bond-dependent coefficient and was proposed to be set as 0.5, E_f is the modulus of elasticity of FRP reinforcement and E_s is the modulus of elasticity of steel reinforcement. Theriault and Benmokrane [78] and Masmoudi et al. [56] compared Eq. (3) with further experimental results and consequently suggested the value of ψ_d to be equal to 0.6, so as to achieve good agreement with the experimentally obtained flexural responses. Bischoff and Gross [15] recommended the value of ψ_d to be evaluated as $0.2\rho_t/\rho_b$, where ρ_t is the FRP tension reinforcement ratio and ρ_b is FRP balanced reinforcement ratio. On the other hand, Bischoff and Gross [15] further suggested Eq. (5) for computing the effective moment of inertia, where ψ_f is equal to 0.44 for FRP-RC beams.

$$I_e = \frac{I_{cr}}{1 - \psi_f \left(1 - \frac{I_{cr}}{I_g}\right)\left(\frac{M_{cr}}{M_a}\right)^2} \leqslant I_g \tag{5}$$

It is interesting to note that in the 2006 version of ACI-440, Eq. (3) and Eq. (4) were recommended with the value of ψ_b suggested to be equal to 0.5 for all types of FRP reinforcement; whereas in the 2015 version of ACI-440, Eq. (5) was recommended with the value of ψ_f suggested to be equal to $(1.72–0.72M_{cr}/M_a)$. The accuracy of using the effective moment of inertia to predict deflections of FRP-RC beams is highly dependent on adopted values of the empirical coefficients. More complicated expressions of the coefficients have been put forward by Mousavi and Esfahani [61], who performed regression analysis of load test results of 55 FRP-RC beams from the literature.

2.2. Theoretical tension-stiffening model

As discussed above, different bond stress-slip laws were employed by various researchers [55,44,21] to derive theoretical tension-stiffening models for RC flexural members. However, there are commonly encountered challenges in the development of tension-stiffening model or moment-curvature relation for FRP-RC beams. Since the bond characteristics of FRP reinforcement and steel reinforcement are different, the theoretical models for conventional steel RC beams are not directly applicable to FRP-RC beams. Research had been performed previously on using more realistic yet complicated bond laws to derive tension-stiffening models for RC axial tension member. For example, Salem and Maekawa [75] used a bond slip law described by logarithmic curves and introduced the bond deterioration zone to account for localized damage in their derivation of tension-stiffening model for axial members. Noh [71] employed a bond slip law with curvilinear ascending and descending branches to derive tension-stiffening model for RC panels. Lee et al. [52] considered the post-yield behaviour and rupture criterion of reinforcing bars in axial members. These close-form models have predicted well the stiffness and deformations of steel RC members. However, it must be pointed out that the tension-stiffening models for axial tension members are not the same as those for flexural members, due mainly to the absence of curvature effect in axial elements, which will be later explained.

As far as the tension-stiffening model for FRP-RC members is concerned, Sooriyaarachchi et al. [77] conducted experimental study of FRP-RC tensile specimens and explored the feasibility of adapting tension-stiffening models for steel RC members to FRP-RC members. Baena et al. [7] referred to the bond law by Eligehausen et al. [25] and proposed a tension-stiffening model for FRP-RC members subjected to axial tension. Mazaheripour et al. [60] employed multi-linear bond stress-slip relation in combination with exponential functions for describing the spatial variations of bond slip along different stages of debonding, and derived a theoretical tension-stiffening model. The model is comprehensive and is applicable to hybrid FRP and steel reinforced normal concrete and steel fibre-reinforced concrete members. However, as discussed above, the tension-stiffening models for axial FRP-RC members cannot be directly applied to flexural FRP-RC members. Such curvature effect is illustrated with a beam section as shown in Fig. 1. Even if the beam is subjected to pure bending, the intact concrete between cracks would sustain a shearing effect that contributes to the tension-stiffening of the member. This is visualized by considering the concrete element in Fig. 1. When subjected to curvature, the top and bottom fibres of the concrete element would deform to different lengths. In the cross-section in Fig. 1, the concrete element is depicted as a slice, over which interfacial shear stress is developed to equilibrate the difference in tension forces across the vertical height of the concrete element. Therefore, dedicated research on the tension-stiffening phenomenon in flexural FRP-RC members is necessary, as aimed in this study.

3. Constitutive model for finite element analysis

3.1. Model for concrete

Concrete is modelled as a biaxial material with the tensile and compressive strengths in the principal directions determined from the biaxial strength envelope formulated by Kupfer and Gerstle [43]. The dual-directional fixed smeared crack model is adopted [31,76,23]. Before cracking, the principal material axes coincide with the principal directions. After cracking, the principal material axes are frozen with the major and minor principal axes set respectively as being orthogonal and tangential to the crack plane. The attainment of cracking tensile strain and fracture energy of concrete, whichever is greater after transforming in terms of tensile stress, is adopted as the cracking criterion [68,54]. Through the use of equivalent uniaxial strains that incorporate the Poisson effect, the biaxial behaviour of concrete can be considered in terms of two independent uniaxial stress-strain relations [24]. The equivalent uniaxial strains are computed from the principal strains as given by the following equations, which cater for the interaction between two principal axial directions [54,84].

$$\varepsilon_{e1} = \frac{1}{1 - \nu_1\nu_2}(\varepsilon_1 + \nu_2\varepsilon_2) \tag{6a}$$

$$\varepsilon_{e2} = \frac{1}{1 - \nu_1\nu_2}(\varepsilon_2 + \nu_1\varepsilon_1) \tag{6b}$$

where ε_{e1} and ε_{e2} are the equivalent uniaxial strains, ε_1 and ε_2 are the principal strains, ν_1 and ν_2 are the Poisson's ratios, and subscripts 1 and 2 denote quantities in the major and minor principal axes, respectively. Through the notion of equivalent uniaxial strains, each of the principal stresses σ_1 and σ_2 can be represented as a single variable function of ε_{e1}

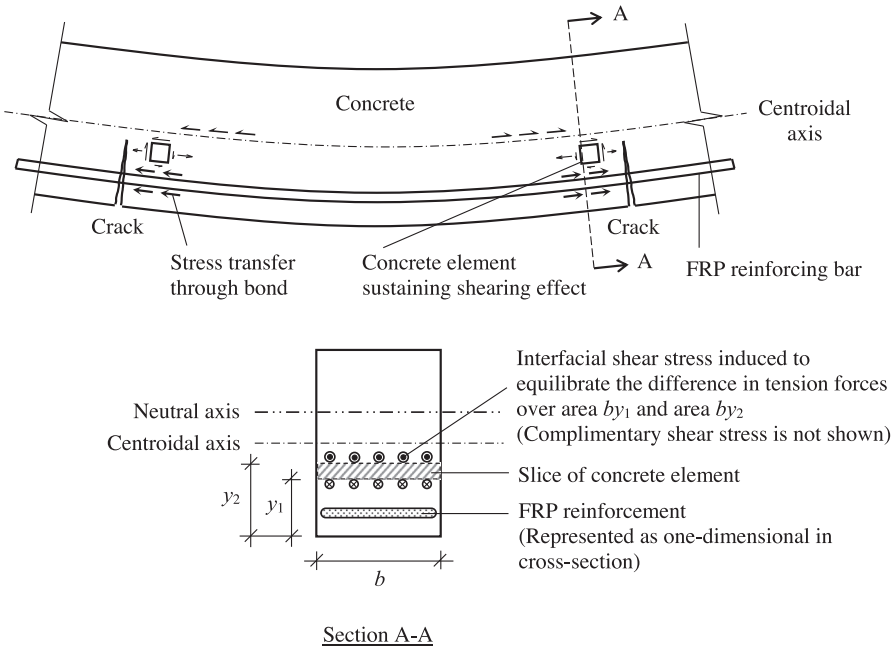

Fig. 1. Curvature effect on tension-stiffening.

and ε_{e2}, respectively.

Along the principal axes with respect to the equivalent uniaxial representation, the stress-strain relation of concrete in compression follows that proposed by Saenz [73], whereas the stress-strain relation of concrete in tension is according to that proposed by Guo and Zhang [36]. Eq. (7) expresses the Saenz's equation that describes the relationship between concrete compressive stress σ_c and concrete compressive strain ε_c. In this equation, E_0 is the initial elastic modulus, E_{co} is the secant modulus at peak compressive stress, and ε_{co} is the strain at peak compressive stress.

$$\sigma_c = \frac{E_0 \varepsilon_c}{1 + \left(\frac{E_0}{E_{co}} - 2\right)\left(\frac{\varepsilon_c}{\varepsilon_{co}}\right) + \left(\frac{\varepsilon_c}{\varepsilon_{co}}\right)^2} \tag{7}$$

Eq. (8) expresses the equation given by Guo and Zhang [36], where f_{to} is the peak tensile stress, and ε_{to} is the strain at peak tensile stress.

$$\sigma = f_{to}\left[1.2\left(\frac{\varepsilon}{\varepsilon_{to}}\right) - 0.2\left(\frac{\varepsilon}{\varepsilon_{to}}\right)^6\right] \text{for } \varepsilon \leqslant \varepsilon_{to} \tag{8a}$$

$$\sigma = \frac{f_{to}\left(\frac{\varepsilon}{\varepsilon_{to}}\right)}{0.312 f_{to}^2\left(\frac{\varepsilon}{\varepsilon_{to}} - 1\right)^{1.7} + \left(\frac{\varepsilon}{\varepsilon_{to}}\right)} \text{for } \varepsilon > \varepsilon_{to} \tag{8b}$$

The principal stresses (or more precisely, the stresses along the directions of principal material axes) σ_1 and σ_2 are obtained by substituting the corresponding equivalent uniaxial strain into the respective stress-strain relation of Eq. (7) or (8), so that the secant moduli E_{c1} and E_{c2} can be respectively evaluated as $\sigma_1/\varepsilon_{e1}$ and $\sigma_2/\varepsilon_{e2}$. The constitutive matrix $[D_c']$ of concrete element in the local coordinate system is formulated as per Darwin and Pecknold [24], as given by:

$$[D_c'] = \frac{1}{1 - \nu_1\nu_2}\begin{bmatrix} E_{c1} & \nu_2 E_{c1} & 0 \\ \nu_1 E_{c2} & E_{c2} & 0 \\ 0 & 0 & (1 - \nu_1\nu_2)G \end{bmatrix} \tag{9}$$

In Eq. (9), for uncracked concrete, the Poisson's ratios ν_1 and ν_2 can be taken as the initial Poisson's ratio ν_0. For cracked concrete, the Poisson's ratio along the major principal material axis is taken as zero, and that along the minor principal material axis is dependent on the biaxial stress state as follows. If the minor principal material axis is in tension, ν_2 is taken as ν_0; whereas if the minor principal material axis is in compression, ν_2 is evaluated per Eq. (10) recommended by Darwin and Pecknold [24]. In any case, the Poisson's ratio is no greater than 0.5 for incompressible material.

$$\nu_2 = 0.2 + 0.4\left(\frac{\sigma_1}{f_t}\right)^4 + 0.6\left(\frac{\sigma_2}{f_c}\right)^4 \leqslant 0.5 \tag{10}$$

Regarding the element coordinates, it should be noted that the local coordinate system follows the principal material axes as discussed above. Since the directions of principal material axes are fixed upon cracking, shear stresses can develop in cracked concrete elements. In Eq. (9), G denotes the shear modulus. Before cracking, the shear modulus is taken as the initial elastic shear modulus $G_0 = E_0/2(1 + \nu_0)$. After cracking, the shear modulus is taken as βG_0, where β is a dimensionless shear retention factor to account for the effect of aggregate interlock as expressed in Eq. (11) [38,49]. In the equation, β_0 can be taken as 0.4, as suggested by Walraven [80] based on test results of shear transfer.

$$\beta = \beta_0\left(1 - \frac{\varepsilon_{e1} - \varepsilon_{t0}}{30\varepsilon_{t0}}\right)^2 \tag{11}$$

The above material modelling of concrete is implemented with the use of plane stress constant strain triangular finite elements. The constitutive matrix $[D_c]$ of concrete in the global coordinate system is obtained by coordinate transformation.

$$[D_c] = [T]^T[D_c'][T] \tag{12a}$$

$$[T] = \begin{bmatrix} c^2 & s^2 & cs \\ s^2 & c^2 & -cs \\ -2cs & 2cs & c^2 - s^2 \end{bmatrix} \tag{12b}$$

where $[T]$ is the transformation matrix, c denotes $\cos\theta$, s denotes $\sin\theta$, and θ is the angle between the global and the local coordinate systems.

3.2. Model for FRP reinforcement

The FRP reinforcement is regarded as behaving in a linearly elastic manner up to failure. The compressive strength of FRP reinforcement is generally lower than the tensile strength [41]. Therefore, the stress-strain relations of FRP reinforcement subjected to tension and subjected to compression are considered separately. Denoting E_{ft} and E_{fc} be respectively the modulus of elasticity of FRP reinforcement under tension and compression, f_{fut} and f_{fuc} be respectively the ultimate tensile and compressive strengths of FRP reinforcement, the constitutive modelling of FRP reinforcement is formulated as follows:

$$\text{Under tension, } \sigma = \begin{cases} E_{ft}\varepsilon \\ 0 \end{cases} \text{ for } \begin{cases} \varepsilon \leqslant f_{fut}/E_{ft} \\ \varepsilon > f_{fut}/E_{ft} \end{cases} \tag{13a}$$

$$\text{Under compression, } \sigma = \begin{cases} E_{fc}\varepsilon \\ 0 \end{cases} \text{ for } \begin{cases} \varepsilon \leqslant f_{fuc}/E_{fc} \\ \varepsilon > f_{fuc}/E_{fc} \end{cases} \tag{13b}$$

FRP materials exhibit brittle behaviour. Beyond reaching the ultimate tensile or compressive strength, the FRP reinforcement is considered as failed, and the stiffness will be assigned an extremely small value to while the element topology and connectivity with the bond interface element are preserved. The above material modelling of FRP reinforcement is implemented with the use of two-node discrete bar finite elements. The constitutive matrix of FRP reinforcement $[D_f']$ in the local coordinate system is formulated from the secant modulus E_f and is given by Eq. (14), and then the constitutive matrix $[D_f]$ of FRP reinforcement in the global coordinate system is obtained by coordinate transformation.

$$[D_f'] = \begin{bmatrix} E_f & 0 & 0 \\ 0 & 0 & 0 \\ 0 & 0 & 0 \end{bmatrix} \tag{14}$$

3.3. Model for bond

The bond between FRP reinforcing bar and concrete is modelled with the use of bond interface elements with duplicated nodes, each represents the degrees of freedom for FRP reinforcement and the degrees of freedom for concrete, respectively. The difference in displacements among the duplicated nodes in the longitudinal direction of FRP reinforcement represents the bond slip. The same technique has been applied to the modelling of steel RC elements by Ng et al. [66,67]. The concrete-FRP reinforcement bond behaviour has been studied by various researchers such as Cosenza et al. [22], Achillides [4], Focacci et al. [30], Baena et al. [6], Mazaheripour et al. [57–59], Pepe et al. [72], Lin and Zhang [53], Fava et al. [26] and Yan et al. [81]. A number of bond stress-slip models have been put forward based on pull-out test results of FRP reinforcement bar. For example, the bond model by Cosenza et al. [22] consists of nonlinear ascending branch and linear descending branch with cut-off equal to the frictional resistance of bond. The bond model is formulated as:

$$\frac{\tau}{\tau_p} = (1 - e^{-s/s_r})^r \text{ for } s \leqslant s_r \tag{15a}$$

$$\frac{\tau}{\tau_p} = 1 - p\left(\frac{s}{s_r} - 1\right) \text{ for } s_r < s \leqslant s_f \tag{15b}$$

$$\tau = \tau_f \text{ for } s > s_f \tag{15c}$$

where τ is the bond stress, s is the bond slip, τ_p is the peak bond stress, s_r is the slip at peak bond stress, r is the exponential index of ascending curve, p is a parameter for softening behaviour of bond, s_f is the slip at transition between softening and remaining frictional resistance of bond, and τ_f is the frictional resistance of bond. The valuation of parameters is based on curve-fitting of experimental data. As examples of parameter values, for sand particles-coated glass fibre-reinforced polymer bars, the average values of s_r, r and p reported by Cosenza et al. [22] were 0.07, 0.14 and 3.11, respectively. The frictional resistance of bond is taken as $0.3(f_c)^{0.5}$ and the initial bond stiffness is taken as 200 MPa/mm which was approximately the average value measured from pull-out tests by Mazaheripour et al. [57,59].

Upon bond slip occurs, the bond stress τ is obtained by substituting the bond slip s into Eq. (15) and the secant bond stiffness k_b is evaluated as τ/s. The above material modelling of concrete-FRP reinforcement bond is implemented with the use of four-node Goodman-type bond interface finite elements with infinitesimal thickness [34]. Each element has two duplicated nodal pairs that share the same un-deformed coordinates but possess independent degrees of freedom to cater for bond slip. The bond element stiffness matrix $[K_b']$ in the local coordinate system is derived as:

$$[K_b'] = \begin{bmatrix} K_{11}' & K_{12}' \\ K_{21}' & K_{22}' \end{bmatrix} \tag{16}$$

in which the submatrices are given by:

$$[K_{11}'] = [K_{22}'] = \frac{p_f a}{3}\begin{bmatrix} 2k_b & 0 & k_b & 0 \\ 0 & 2k_n & 0 & k_n \\ k_b & 0 & 2k_b & 0 \\ 0 & k_n & 0 & 2k_n \end{bmatrix} \tag{17a}$$

$$[K_{12}'] = [K_{21}'] = \frac{p_f a}{3}\begin{bmatrix} -2k_b & 0 & -k_b & 0 \\ 0 & -2k_n & 0 & -k_n \\ -k_b & 0 & -2k_b & 0 \\ 0 & -k_n & 0 & -2k_n \end{bmatrix} \tag{17b}$$

In the above, p_f is the total perimeter of the FRP reinforcing bars, a is half of the length of bond element along its longitudinal direction, k_n is the normal stiffness between concrete and FRP reinforcement. Suppose k_c is the contact stiffness of concrete and k_f is the contact stiffness of FRP reinforcement at the concrete-FRP interface evaluated based on the bearing area, the normal stiffness k_n is computed as:

$$k_n = \left(\frac{1}{k_c} + \frac{1}{k_f}\right)^{-1} \tag{18}$$

Subsequently, the bond element stiffness matrix in the global coordinate system can be obtained by coordinate transformation with respect to the direction cosine and direction sine. For brevity, the mathematical formulae for coordinate transformation are not contained here. Readers may consult dedicated text [8] for the detailed formulation.

3.4. Numerical approach

The constitutive models presented in the foregoing have been formulated in the nonlinear finite element programme developed and reported elsewhere [68,70]. Direct iteration is adopted for the solution process based on secant stiffness of the elements. The sign convention is taken as tension-positive and compression-negative. The loading is applied in small increments as prescribed displacement, with the full range of loading divided into approximately 100 incremental steps. In each incremental step, direct iteration is performed until the change in secant modulus in every finite element relative to the preceding iteration is no greater than 2%. Specific modules for mesh generation and for capturing the tension stress field of structural members have been computerised [65,48] to automate the pre-processing and post-processing. The accurate and reliable performance of the nonlinear finite element programme in analyzing RC structural members have been fully verified and demonstrated in the previous publications [46,47,54,67,70]. Detailed description of the capturing of tension stress field, which is an essential step for the derivation of tensile stress block, is contained in the next section.

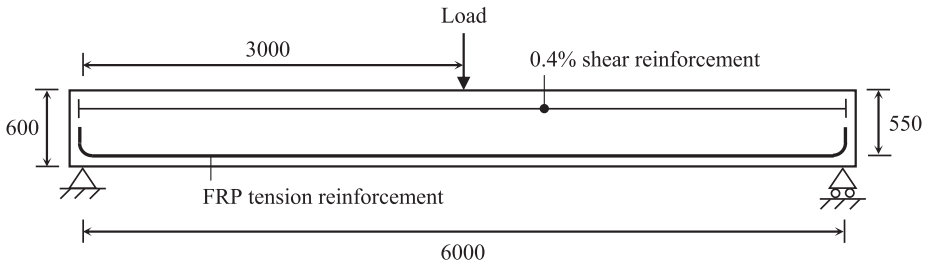

(a) Single point load configuration

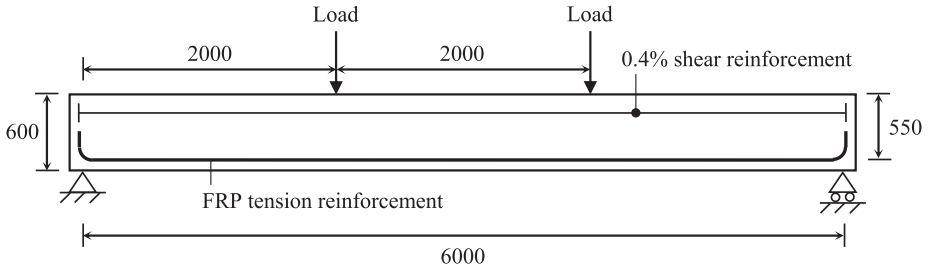

(b) Two-point load configuration

Fig. 2. Layout of FRP-RC beams (dimensions in mm).

4. Determination of tensile stress block

4.1. Finite element simulation of FRP-RC beams

A series of simply-supported FRP-RC beams with different reinforcement ratios are analyzed by means of finite element method to reflect their tension-stiffening behaviour. The beams have uniform cross-section of 300 mm (breadth) × 600 mm (depth). The effective depth from top of beam to the centroid of tension reinforcement is 550 mm and the span is 6000 mm. The FRP tension reinforcement ratio ρ_{ft} varies among 0.5%, 1.0%, 1.5% and 2.0%. Steel shear reinforcement is provided with the ratio fixed at 0.4%. The shear reinforcement is modelled using the smeared approach (unlike the tension reinforcement which is modelled using the discrete approach) where its stiffness is integrated with the concrete elements. The beams are either subjected to single point load at its mid-span or two-point load at its third points. Fig. 2 depicts the layout of the beams. The beams are discretised into ten layers of finite elements over the beam height in the mesh generation process. To verify the adequacy of the mesh fineness, the analysis has been repeated with the beam height discretised into eight, ten and twelve layers of finite elements. The resulting load versus deflection responses are basically identical (therefore only the load-deflection response from a single mesh fineness is shown in Fig. 3) and the resulting tension stress fields are highly similar. For illustration, the stress contours in direction of major principal material axis for the beam with 0.5% FRP reinforcement ratio subject to two-point load from different mesh refinement at 25% of peak load are depicted in Fig. 4. Dedicated studies were also performed by Ng et al. [68] and Ma et al. [54], where convergent results of load–displacement response and crack patterns were obtained. Overall speaking, the mesh fineness has attained convergence and the computed structural response is not altered by further reducing the mesh size.

The properties of materials considered are typical values as follows. For concrete, the uniaxial tensile strength f_t and uniaxial compressive strength f_c are respectively 3.0 MPa and 30.0 MPa. The initial elastic modulus E_0 and initial Poisson's ratio ν_0 are 30.0 GPa and 0.2, respectively. For FRP reinforcement, the ultimate tensile strength f_{fut} and

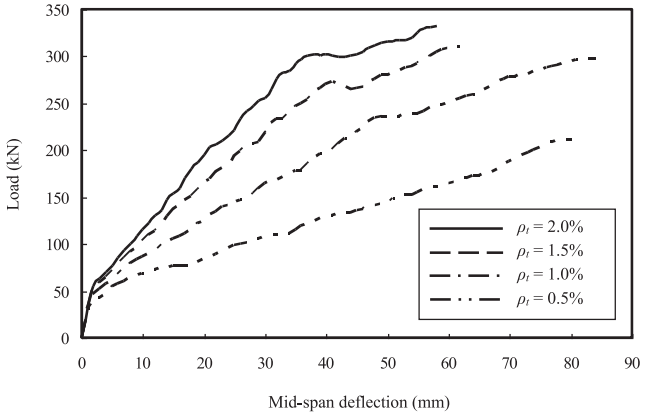

(a) Beams subjected to single point load

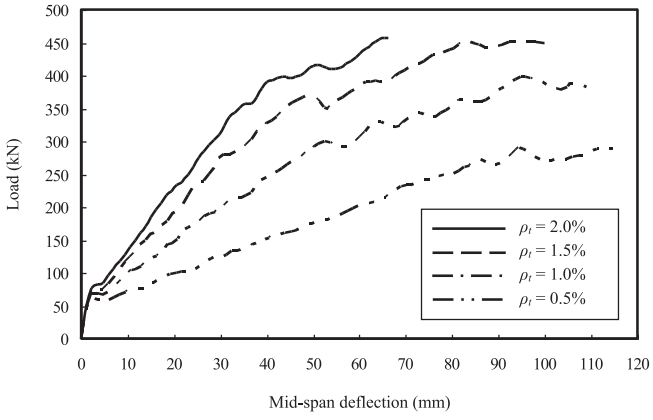

(b) Beams subjected to two-point load

Fig. 3. Load-deflection curves from finite element analysis.

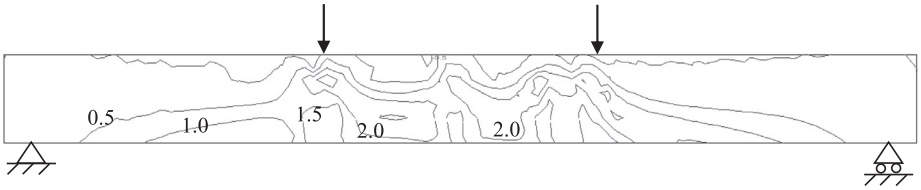

(a) Beam height discretized into eight layers of finite elements

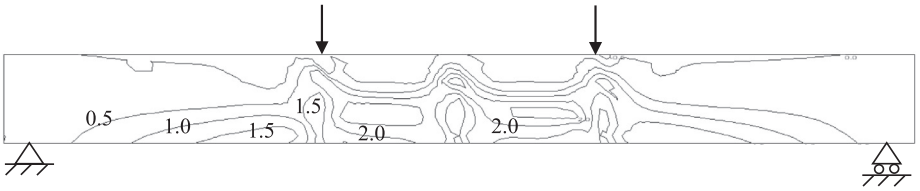

(b) Beam height discretized into ten layers of finite elements

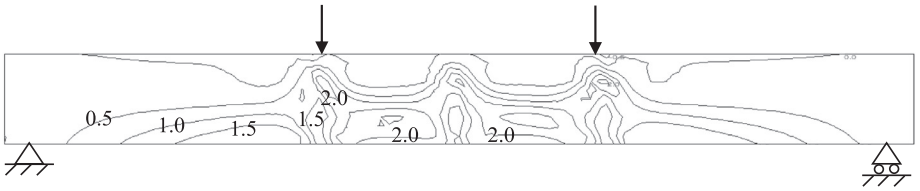

(c) Beam height discretized into twelve layers of finite elements

Fig. 4. Stress contours in direction of major principal material axis (unit in MPa).

tensile elastic modulus E_{ft} are respectively 700 MPa and 50 GPa (typical values for glass fibre-reinforced polymer). For the bond between concrete and FRP reinforcement, the bar diameter and total perimeter are back-calculated from geometry based on the assumption that the required reinforcement area is provided by two reinforcing bars of suitable size; the parameters s_r, r and p are taken as 0.07, 0.14 and 3.11, respectively. The peak bond stress τ_p is taken as $2f_c^{0.5}$ and s_f is taken as s_r.

The load versus mid-span deflection curves of the beams analyzed are plotted in Fig. 3. For beams subject to two-point load, the sum of applied loads at the two loading points is plotted. Typically, the load-deflection curves are linear from the beginning to approximately 15% of the peak load. Afterwards, the flexural stiffness decreases due to cracking of the beams. Upon further increase in applied load, the gradient of the curve becomes fairly constant. At approximately 80% to 85% of the peak load, the beams soften and may exhibit a moderate (1% to 4%) drop of load resistance, as a result of extensive cracking of concrete in the tension zone. Afterwards, the load resistance regain and further increase at a more gentle gradient. This is followed by brittle rupture of the FRP reinforcement at the peak load, and the beams lose the flexural capacity. Among all beams, the peak load increases with the tension reinforcement ratio, and the peak load of beams subjected to single point load is approximately 67% to 72% of that of beams subjected to two-point load.

To illustrate the computed structural behaviour, Fig. 5 displays the crack pattern, reinforcement stress distribution, and bond slip variation for the beam with ρ_{ft} = 0.5% subjected to two-point load at 25% of peak load. Flexural crack first formed at mid-span and hence the cracks are more developed there, as shown in Fig. 5(a). Both the reinforcement stress distribution as shown in Fig. 5(b) and the variation of bond slip along the FRP reinforcement as shown in Fig. 5(c) correspond to the crack locations. At every cracked section, the reinforcement stress reaches a local maximum, and the bond slip exhibits reversal in direction. The above indicates the validity of the finite element analysis results.

4.2. Tension stress field from finite element analysis

The procedures for derivation of the tensile stress block for steel RC beams in Ng et al. [64] with proven rationality and reliability are adopted in this study. Basically, the procedures are to determine the representative relationship between tensile stresses and tensile strains across different beam sections and under different service load levels. As the first step, the tension stress field for each analyzed beam is obtained. At different sections along the FRP-RC beam, the variations of tensile stresses in concrete with the distance from neutral axis are obtained from the finite element analysis. These variations of tensile stresses can be consolidated to the tensile stress block, by plotting the tensile stress against the theoretical tensile strain. Here, the theoretical tensile strain refers to tensile strain value evaluated from the effective flexural stiffness of the beam sections, in other words, with the cracks smeared so that the flexural stiffness of the beam section changes smoothly with the mean curvature. In theory, the theoretical tensile strain may be evaluated as the mean curvature ϕ multiplied by the depth from neutral axis z. However, for a cracked beam, the curvature fluctuates between adjacent cracks. To evaluate the mean curvature of a beam section, a short region of the beam extending one beam depth from each side of the section is considered. The local fluctuation of curvature over the short region with length equal to two times the beam depth is smoothed. Firstly, the deflected shape within the short region is fitted with a cubic polynomial curve. Secondly, the cubic polynomial is differentiated twice with respect to the length to obtain the smoothed curvature value as the mean curvature at the beam section considered. Thirdly, the theoretical tensile strain is obtained as the product of mean

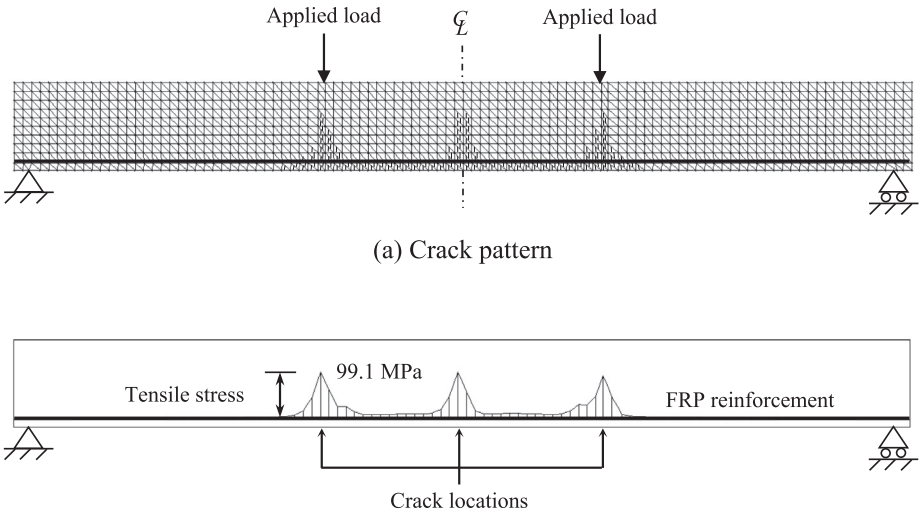

Fig. 5. Crack pattern and stress distributions.

curvature and neutral axis depth. This yields the diagram of concrete tensile stress versus the theoretical tensile strain.

Dependent on whether a section is cracked or uncracked as well as its distance from the nearest cracked section, the variation of the tensile stress with the theoretical tensile strain is rather different along the beam. Fig. 6 schematically illustrates the stress and strain distributions in the tension zone of beam. To obtain a representative variation of tensile stresses, the mean tensile stress is evaluated as the smoothed tensile stress with local fluctuations in the longitudinal direction removed by considering a truncated block of the cracked beam with length equal to the crack spacing. Suppose there are totally *n*-longitudinal sections of finite elements within the block. Firstly, the variations of the tensile stress from finite element analysis with the theoretical tensile strain are plotted for the *n* sections within the block. Secondly, the mean tensile stress at each theoretical tensile strain level is evaluated as the root-mean-square of the tensile stress values of the *n* sections at the theoretical tensile strain level being considered. Root-mean-square is adopted as the mean because this will result in the same strain energy after the stress smoothing. For a beam with multiple cracks of different heights, the theoretical tensile strain contours would be a family of undulating curves, as depicted in Fig. 6.

The diagram of mean tensile stress versus the theoretical tensile strain are obtained using the above method for each beam at each load level equal to 15%, 20%, 30%, 40%, 50% and 60% of the respective

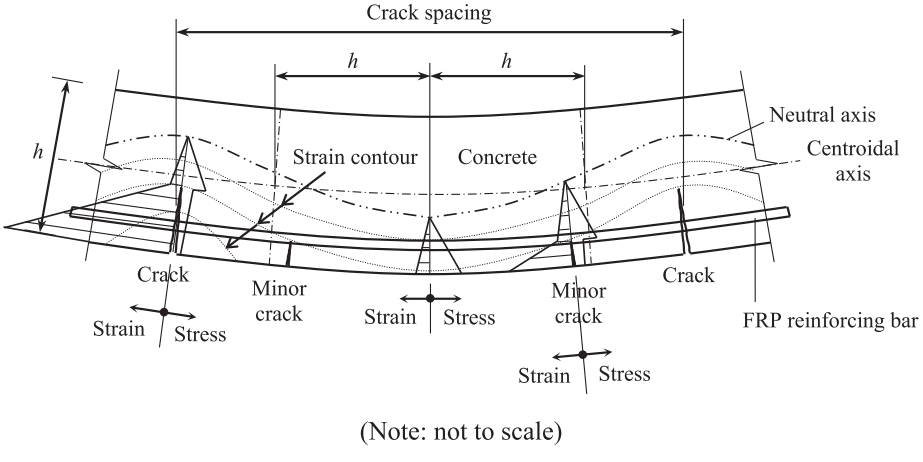

Fig. 6. Stress and strain distributions in tension zone.

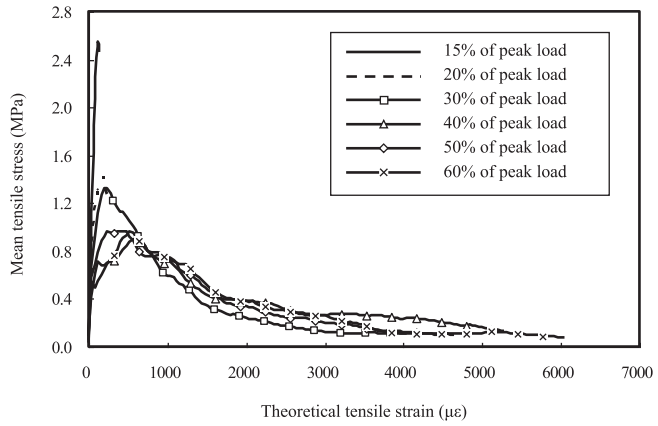

(a) Beams subjected to single point load

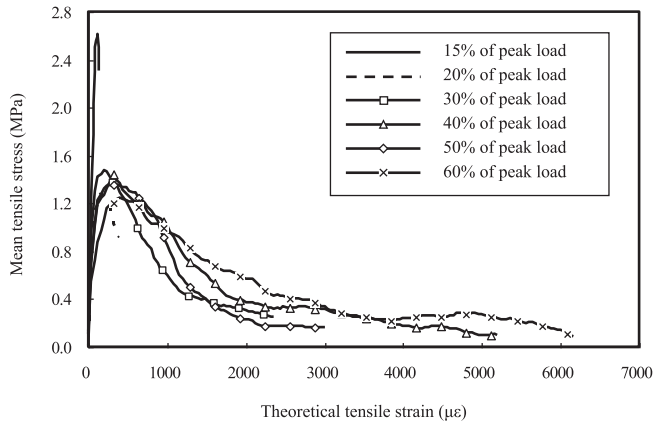

(b) Beams subjected to two-point load

Fig. 7. Diagram of mean tensile stress versus theoretical tensile strain.

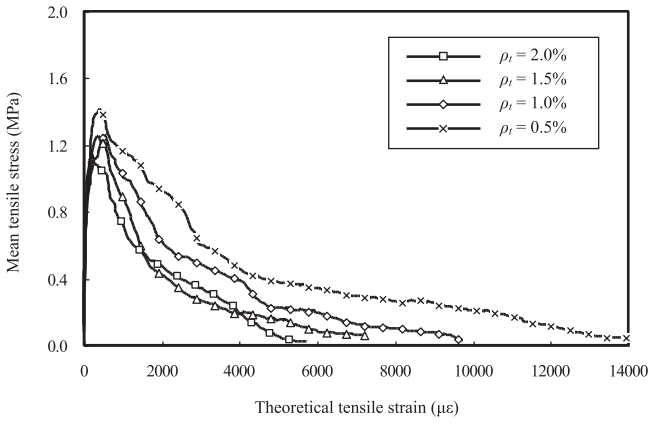

(a) Beams subjected to single point load

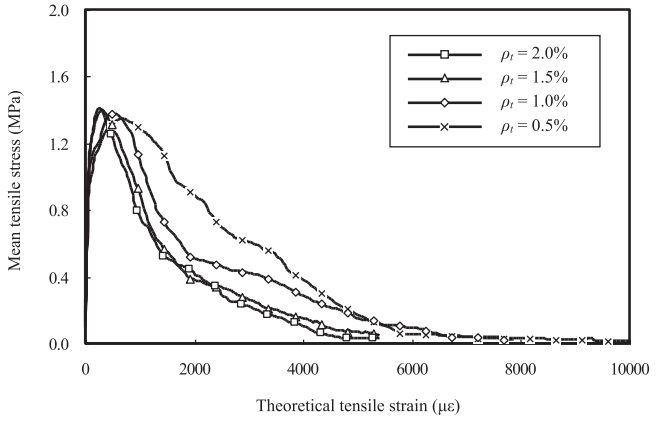

(b) Beams subjected to two-point load

Fig. 8. Averaged diagrams of mean tensile stress versus theoretical tensile strain.

peak load. These load levels encompass scenarios ranging from slightly loaded condition to the entire service condition. To illustrate the result, the mean tensile stress versus the theoretical tensile strain diagrams for the FRP-RC beams with ρ_{ft} equal to 1.5% subject to single point load and two-point load are plotted in Fig. 7. It can be seen that at 15% of peak load (basically uncracked), the mean tensile stress-theoretical tensile strain curve is a straight line ascending from the origin to approach the tensile strength of concrete (due to very slight cracking, the mean tensile stress does not reach the tensile strength but starts to descend; nevertheless, if the element stresses are captured at the load level right before first cracking, the resulting curve will only be a straight line from the origin to very close to the tensile strength). At 20% of peak load, when the beam has cracked slightly, the linear ascending branch of the curve reaches a stress level lower than the previous peak value, and there is a short descending branch.

From 30% to 60% of the peak load, where the beam is under service regime, the tension-stiffening phenomenon is more apparent. At 30% of peak load, the ascending branch becomes more nonlinear and it reaches a peak value approximately equal to less than half or half of the tensile strength of concrete, while the descending branch has the geometry of a concave curve and ends at a theoretical tensile strain of one order larger than the cracking strain. The trend continues for higher load levels, with the descending branch extends to form longer tail ending at larger theoretical tensile strain. Attempt is made to combine the four diagrams for 30%, 40%, 50% and 60% of peak load by arithmetic averaging into one single diagram for the post-crack state. Such averaging is performed for all FRP-RC beams in the series. Fig. 8 plots the averaged diagrams, which appear to be affected by the FRP reinforcement ratio (compare the diagrams in the same graph in Fig. 8(a) or Fig. 8(b)) and the type of load (compare the diagrams across different graphs in Fig. 8(a) and Fig. 8(b)). Relatively, the type of load plays a more important role (this will be discussed in greater depth in the subsequent section). From Fig. 8, it can be seen that the diagrams for beams under single point load tend to have slightly lower peaks and longer tails, whereas the diagrams for beams under two-point load tends to have slightly higher peaks and shorter tails.

4.3. Proposed parametrized tensile stress block

As discussed above and shown in Fig. 7, typically the diagram of mean tensile stress versus the theoretical tensile strain before cracking is a straight line from the origin ascending towards the tensile strength of the concrete, while the diagram after cracking comprises a nonlinear ascending branch approaching about half the concrete tensile strength and a nonlinear descending branch in the form of a concave curve with a long tail. These two distinct layouts of the diagrams before and after cracking are shown schematically in Fig. 9(a). For use in deformation analysis of FRP-RC beams, it is proposed to integrate the two distinct layouts of diagrams into one combined tensile stress block, as shown in Fig. 9(b). For simple practical implementation by engineers, the concave curve descending branch is approximated by two straight line segments. Similar approximation of descending branch by multi-linear segments was devised by Barros [9] in the modelling of fibre-reinforced concrete.

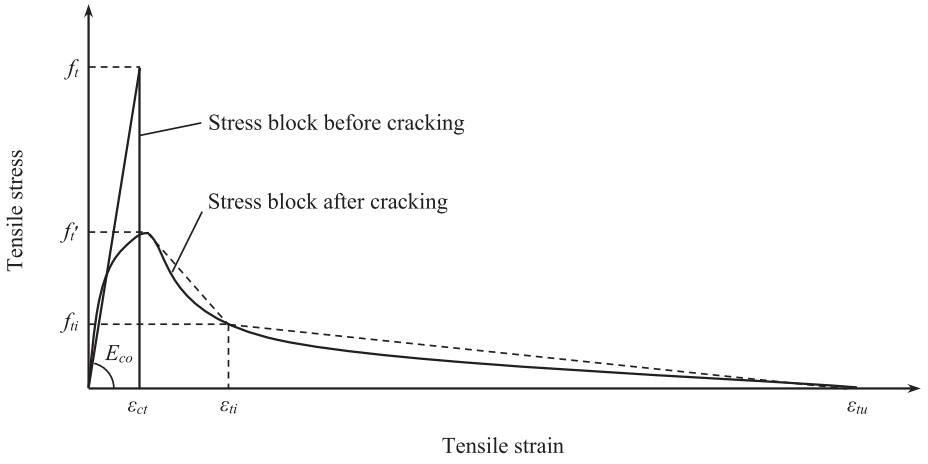

(a) Distinct stress blocks before and after cracking

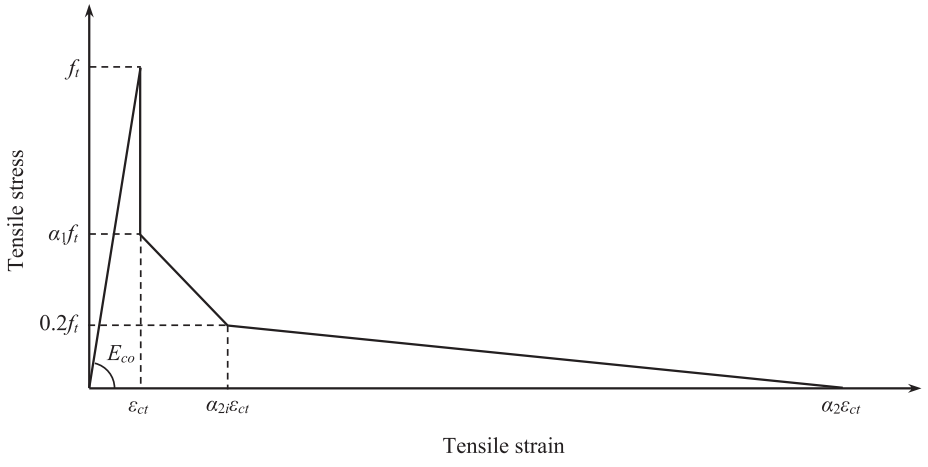

(b) Proposed combined stress block

Fig. 9. Tensile stress block for FRP-RC beams.

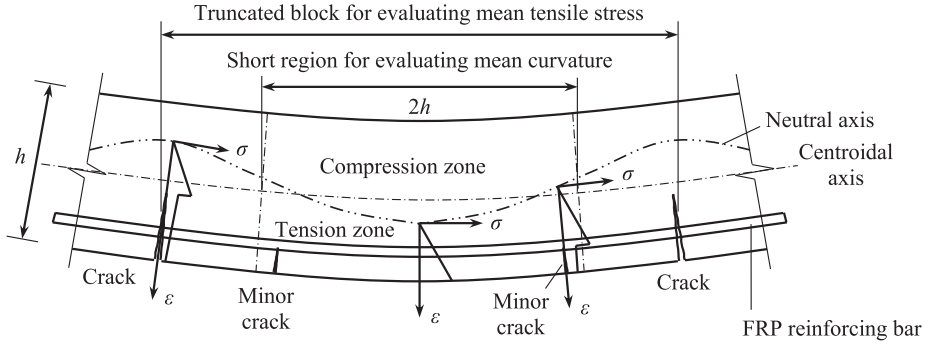

(Note: not to scale)

Fig. 10. Projection of tensile stress block along longitudinal direction.

The proposed combined tensile stress block is a multi-linear diagram. It has a linear ascending branch and a bilinear descending branch. Along the ascending branch, the tensile stress increases linearly from zero to the tensile strength of the concrete f_t at a gradient equal to the initial elastic modulus of concrete. This is followed by an abrupt drop of the tensile stress from f_t to a reduced level denoted as f_t'. Along the descending branch, since the rate of decrease of the concave curve is not constant, an intermediate point is defined so that the curve can be

idealised to two straight line segments. The tensile stress first decreases linearly from f_t' to an intermediate value of $0.2f_t$ at an intermediate tensile strain ε_{ti}, then further decrease linearly from $0.2f_t$ to zero at an ultimate tensile strain ε_{tu}. The values of f_t', ε_{ti} and ε_{tu} are expressed in terms of three dimensionless coefficients, α_1, α_{2i} and α_2, as given by the following equations:

$$f_t' = \alpha_1 f_t \tag{19a}$$

$$\varepsilon_{ti} = \alpha_{2i}\varepsilon_{ct} \tag{19b}$$

$$\varepsilon_{tu} = \alpha_2\varepsilon_{ct} \tag{19c}$$

where ε_{ct} is the tensile strain at which the peak tensile stress occurs and is regarded as the cracking strain. Mathematically, ε_{ct} is computed as f_t/E_{co}. In contrast to the tensile stress block for steel RC beams proposed earlier [64], where the descending branch is linear and the stress block is defined by two parameters namely α_1 and α_2, an additional parameter α_{2i} is introduced to define the tensile stress block for FRP-RC beams that has a bilinear descending branch. Fig. 10 schematically illustrates the projection of tensile stress block in cracked and uncracked sections along the longitudinal direction of a beam. It is seen that due to different ranges of tensile strains at different cracked and uncracked sections, the stress block is projected to different scales. The equations for the proposed tensile stress block are presented below:

$$\sigma = E_0\varepsilon \text{ for } \varepsilon \leqslant \varepsilon_{ct} \tag{20a}$$

$$\sigma = \frac{\alpha_1 f_t(\alpha_{2i}\varepsilon_{ct} - \varepsilon) + 0.2f_t(\varepsilon - \varepsilon_{ct})}{(\alpha_{2i}\varepsilon_{ct} - \varepsilon_{ct})} \text{ for } \varepsilon_{ct} < \varepsilon \leqslant \alpha_{2i}\varepsilon_{ct} \tag{20b}$$

$$\sigma = \frac{0.2f_t(\alpha_2\varepsilon_{ct} - \varepsilon)}{(\alpha_2\varepsilon_{ct} - \alpha_{2i}\varepsilon_{ct})} \text{ for } \alpha_{2i}\varepsilon_{ct} < \varepsilon \leqslant \alpha_2\varepsilon_{ct} \tag{20c}$$

$$\sigma = 0 \text{ for } \alpha_2\varepsilon_{ct} < \varepsilon \tag{20d}$$

The values of α_1, α_{2i} and α_2 may be determined by referring to Fig. 8 for each beam. The obtained values of stress block parameters are listed in Table 1. For beams subjected to single point load, α_1 ranges from 0.39 to 0.47 with a mean of 0.43, α_{2i} ranges from 10.0 to 25.0 with a mean of 16.0, and α_2 ranges from 45.8 to 116.7 with a mean of 69.7. For beams subjected to two-point load, α_1 ranges from 0.45 to 0.47 with a mean of 0.46, α_{2i} ranges from 10.4 to 26.7 with a mean of 15.7, and α_2 ranges from 39.2 to 52.5 with a mean of 45.7. From the numerical values, it is observed that α_1 is not very sensitive to the FRP reinforcement ratio, while both α_{2i} and α_2 decrease when the FRP reinforcement ratio increases. Besides, the type of load has a stronger influence on α_2 than on α_1, while α_{2i} is not sensitive to the type of load.

An attempt is made to generalise the stress block parameters for different structural configurations and load configurations, in order to enhance the applicability of the proposed method for practical usage. Further information regarding the stress block parameters can be revealed by comparing with the parametric values for steel RC beams reported elsewhere [64,66]. From these two references, it was suggested that α_1 can be taken as 0.4 for single point load and 0.5 for two-point load and distributed load. Apparently, α_1 is not influenced by the reinforcement material. From the two references, it was further suggested that α_2 can be taken as 18 for single point load, while α_2 gradually reduces with the shear span for two-point load and reaches a value of 14 for uniformly distributed load. In view of the difference in elastic moduli between steel and FRP, comparison is made after dividing by the modular ratio m_r, which is designated as the ratio of elastic modulus of reinforcement to elastic modulus of concrete. Considering the elastic modulus of steel E_s to be 200 GPa and the typical value of modular ratio for steel RC member to be $E_s/E_c = 6.67$, the above values of α_2 for steel RC beam could be stated as $120/m_r$ and $93/m_r$, in lieu of 18 and 14, respectively. Likewise, considering the typical value of modular ratio for FRP-RC member to be $E_f/E_c = 1.67$ (again, typical value of E_f of glass fibre-reinforced polymer is taken), the above mean values of α_2 for FRP-RC beam could be stated as $116/m_r$ and $76/m_r$, in lieu of 69.7 and 45.7, respectively. It appears possible to unify the expression of α_2 for steel RC and FRP-RC beams, by introducing m_r as the denominator. Besides, there is possible dependence of α_{2i} and α_2 on the FRP tension reinforcement ratio. Further investigation on this aspect to enhance the accuracy of deformation analysis and to extend the applications to other types of FRP (such as carbon fibre and aramid fibre-reinforced polymer) is recommended.

5. Incorporation of tensile stress block in member analysis

The tensile stress block derived in the above is incorporated into member analysis, which is described in this section. There are three basic assumptions made in the analysis: (1) plane sections remain plane after bending; (2) the bond slip between concrete and FRP reinforcement is indirectly accounted for via the tensile stress block; and (3) the cracking criterion of concrete is solely based on the cracking tensile strain. Regarding the second assumption, though the member analysis does not reflect physical slip movement between concrete and FRP reinforcement, the derivation of tensile stress block has taken into account the bond slip as part of the constitutive model. This is because the transfer of tension force between concrete and FRP reinforcement takes place through the bond action, which is characterised by the bond stress-slip relation. Therefore, the effect of bond slip is included in the mechanical model. Regarding the third assumption, uncracked concrete becomes cracked only if the cracking tensile strain is attained. In other words, there is no provision of any shear crack in the model, and the tension cracks (inclusive of flexural tension crack) are fully accountable for the tension-stiffening behaviour of the member. Compared to the nonlinear finite element analysis presented in the preceding section, the member analysis is simpler and more suitable for practical applications.

In conducting the analysis, the structural member is divided into multiple segments. Each segment is treated as a frame element with two nodes, and each node possesses translational and rotational degrees of freedom. The stiffness matrix $[K]$ for each frame element is a 12×12 matrix, which can be simplified to a 6×6 matrix by considering the two-dimensional plane frame instead of the three-dimensional space

Table 1
Parametric values of tensile stress block for FRP-RC beams.

Type of load	ρ_t	f_t' (MPa)	ε_{ti} (με)	ε_{tu} (με)	α_1	α_{2i}	α_2
Single point load	0.5%	1.42	3000	14,000	0.47	25.0	116.7
	1.0%	1.26	2050	8100	0.42	17.1	67.5
	1.5%	1.26	1450	5850	0.42	12.1	48.8
	2.0%	1.17	1200	5500	0.39	10.0	45.8
	Mean values of α_1, α_{2i}, and α_2				0.43	16.0	69.7
Two-point load	0.5%	1.35	3200	6300	0.45	26.7	52.5
	1.0%	1.38	1800	5850	0.46	15.0	48.8
	1.5%	1.40	1300	5100	0.47	10.8	42.5
	2.0%	1.41	1250	4700	0.47	10.4	39.2
	Mean values of α_1, α_{2i}, and α_2				0.46	15.7	45.7

Note: The single point load is applied at mid-span; the two-point load is applied at third points.

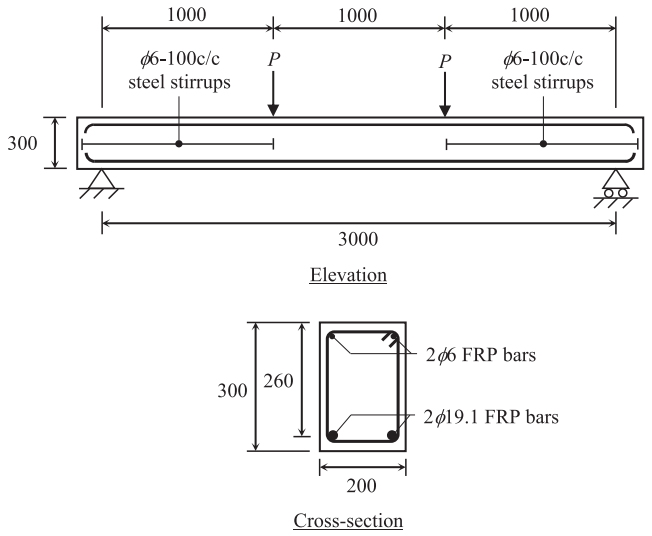

Fig. 11. Layout of beam ISO1 (dimensions in mm).

frame. The formulation of $[K]$ matrix is given by:

$$[K] = \int [B]^T [S][B] dl \tag{21}$$

where $[B]$ is the strain-displacement matrix, $[S]$ is the section stiffness matrix, and the integration is performed over the length of the frame element. The frame element is a Timoshenko-type beam with inclusion of shear deformation in its stiffness matrix. Denote the two nodes of a frame element by node i and node j, at any location within the frame element, the axial strain ε_A, curvature about x-axis κ_x, and curvature about y-axis κ_y can be expressed as:

$$\begin{bmatrix} \varepsilon_A \\ \kappa_y \\ \kappa_x \end{bmatrix} = [B] \begin{bmatrix} \delta_i \\ \delta_j \end{bmatrix} \tag{22}$$

in which $[\delta_i]$ and $[\delta_j]$ are respectively the nodal degrees of freedom at nodes i and j. The section stiffness matrix $[S]$ is given by Eq. (23), where E_c and E_f are respectively the elastic moduli of concrete and FRP reinforcement, dA_c is the part of sectional area being considered, and A_f is the area of FRP reinforcement. It is noteworthy to remark that at sectional level, based on the third assumption above which implies the absence of any shear crack, only the axial translational and rotational degrees of freedom are present in the matrix equation at sectional level for analyzing the tension-stiffening effect.

$$[S] = [S_c] + [S_f] \tag{23a}$$

$$[S_c] = \begin{bmatrix} \int E_c dA_c & \int E_c x dA_c & \int E_c y dA_c \\ \int E_c x dA_c & \int E_c x^2 dA_c & \int E_c xy dA_c \\ \int E_c y dA_c & \int E_c xy dA_c & \int E_c y^2 dA_c \end{bmatrix} \tag{23b}$$

$$[S_f] = \begin{bmatrix} \sum E_f A_f & \sum E_f x A_f & \sum E_f y A_f \\ \sum E_f x A_f & \sum E_f x^2 A_f & \sum E_f xy A_f \\ \sum E_f y A_f & \sum E_f xy A_f & \sum E_f y^2 A_f \end{bmatrix} \tag{23c}$$

To achieve accurate results, the division of member should yield sufficiently short segments, such that the section stiffness matrix can be assumed as constant and representative of the constitutive matrix of each frame element. In this study, the beam is divided into not less than 60 segments, nevertheless, from experience, division of a beam member into 20 segments would already yield satisfactorily accurate results [50,69]. For each of the segments, sectional analysis is employed to determine the stress and deformation states [51]. The section stiffness matrix $[S]$ is assembled based on Eq. (23). It should be noted that following the previous discussions on constitutive model of materials, E_c and E_f are variables dependent on the strain states of the concrete and FRP reinforcement. For concrete in compression, the stress-strain relation as given by Saenz [73] in Eq. (7) is used for evaluating E_c. For concrete in tension, the tensile stress block as formulated in Eq. (20) is used for revaluating E_c. For FRP reinforcement, the stress-strain relation as given in Eq. (13a) or Eq. (13b) is used for evaluating E_f, depending on whether the FRP reinforcement is under tension or compression.

In the solution process of member analysis, an incremental-iterative technique with secant stiffness formulation is adopted. The use of secant stiffness formulation ensures numerical stability at post-crack and post-peak stages of segments. The load is applied in small increments, which theoretically can be in the form of prescribed forces or prescribed displacements at the loading points. In the present study, the load is simulated by means of prescribed displacements. Within each incremental step, an iterative process of solution based on Newton-Raphson's method is adopted. For each segment, the entries of the section stiffness matrix $[S]$ are updated with respect to the computed strain states, and the stiffness matrix of frame element $[K]$ is in turn updated based on the section stiffness matrix, subsequently the updated $[K]$ matrices are assembled into the stiffness matrix of the structural member. Iteration is repeated until the convergence criterion is met, where the changes in the secant stiffness of all frame elements are no greater than 2%. The analysis then proceeds to the next increment step and above numerical procedures are repeated, until the required load level is reached. From the force and displacement results in the series of incremental steps, moment-deflection curve of the beam can be evaluated. The computation procedures presented in the above have been formulated in the nonlinear member analysis programme developed and reported previously [50,69].

6. Analysis of experimental FRP-RC beams

A total of four FRP-RC beams, 2 of which being tested by Benmokrane et al. [11] and 2 of which being tested by Masmoudi et al. [56], are analyzed by means of the equation of effective moment of inertia pursuant to ACI-440 [3], nonlinear finite element analysis, and member analysis using the tensile stress block depicted in the above.

6.1. Beams ISO1 and ISO3 tested by Benmokrane et al. [11]

Beam specimens ISO1 and ISO3 tested by Benmokrane et al. [11] are selected for analysis. Figs. 11 and 12 depict the layout of the beams, whose geometric and material characteristics are summarised in the second and third columns of Table 2. The beams had length of 3300 mm and span of 3000 mm. They were simply supported and subjected to symmetrical two-point loads at third points. The sectional size of beams ISO1 and ISO3 were 200 × 300 mm and 200 × 550 mm (breadth b × depth h), respectively. Both beams were reinforced with two 19.1 mm diameter FRP tension reinforcement and two 6.0 mm diameter FRP compression reinforcement. The surface of the FRP reinforcing bars was finished with a coating of sand particles to improve the bond between concrete and reinforcement. The ultimate tensile strength, ultimate compressive strength, modulus of elasticity under tension, and modulus of elasticity under compression of the FRP reinforcement were respectively 690 MPa, 540 MPa, 45 GPa, and 40 GPa. Steel stirrups of 6 mm diameter at 100 mm spacing were provided within the shear spans of the beams. The stirrups had yield strength of 300 MPa and modulus of elasticity of 200 GPa. The concrete had compressive strength of 43 MPa and modulus of elasticity of 33 GPa.

The variations of flexural moment in the pure bending zone with deflection at mid-span of beams ISO1 and ISO3 obtained from experiment are depicted in Figs. 13 and 14. According to the reported results by Benmokrane et al. [11], the failure mode of beam ISO1 was shear-compression failure of concrete, and the failure mode of beam ISO3 was tensile rupture of FRP reinforcement. In the same figures, the moment-deflection responses evaluated using the ACI-440 equation of effective

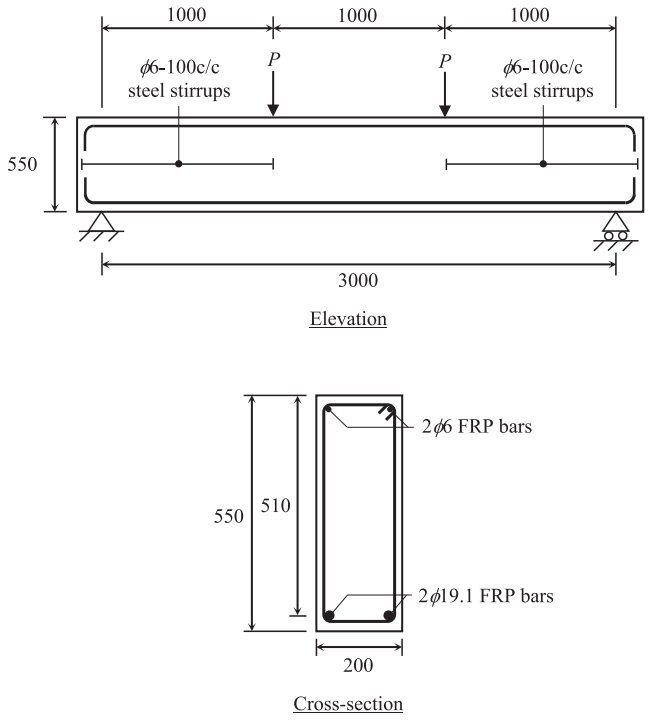

Fig. 12. Layout of beam ISO3 (dimensions in mm).

Table 2
Geometric and material characteristics of FRP-RC beam specimens.

Beam specimen	ISO1	ISO3	CB2B-1	CB3B-1
Breadth of beam section, b (mm)	200	200	200	200
Depth of beam section, h (mm)	300	550	300	300
Effective depth, d (mm)	260	510	253	253
Span length, L (m)	3.0	3.0	3.0	3.0
Shear span, L_1 (m)	1.0	1.0	1.25	1.25
FRP tension reinforcement ratio, ρ_{ft} (%)	1.10	0.56	0.56	0.91
Compressive strength of concrete, f_c (MPa)	43	43	52	52
Modulus of elasticity of concrete, E_0 (GPa)	33	33	33	33
Ultimate tensile strength of FRP, f_{fut} (MPa)	690	690	773	773
Ultimate compressive strength of FRP, f_{fuc} (MPa)	540	540	–	–
Modulus of elasticity of FRP in tension, E_{ft} (GPa)	45	45	38	38
Modulus of elasticity of FRP in compression, E_{fc} (GPa)	40	40	–	–

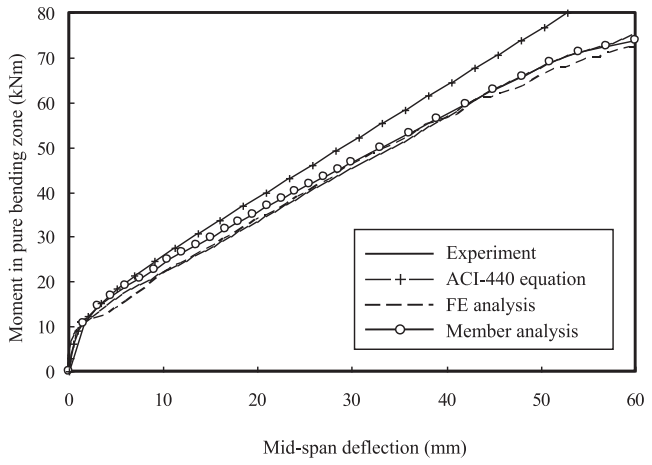

Fig. 13. Moment-deflection curves of beam ISO1.

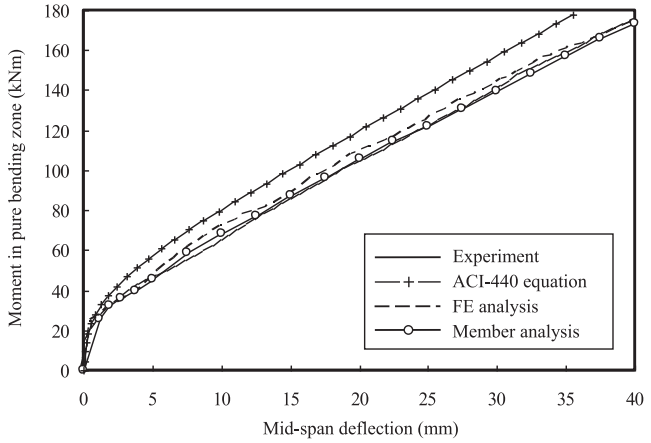

Fig. 14. Moment-deflection curves of beam ISO3.

moment of inertia and finite element analysis are plotted. It can be seen that after cracking, at given level of flexural moment, the calculated deflection per ACI-440 is notably smaller than the experimental deflection. In other words, the ACI-440 provisions underestimate the flexural deflection. This is non-conservative from the serviceability assessment viewpoint. For beam ISO3 whose FRP tension reinforcement ratio ρ_{ft} is lower than beam ISO1, the underestimation of deflection is more pronounced. The same observation is also noted from the other two beams tested by Masmoudi et al. [56], as detailed later. Nevertheless, the accuracy could be improved by suitable adjustment of the empirical coefficient in Eq. (3).

Since both beams ISO1 and ISO3 are subjected to two-point load applied at third points, the load configuration is identical to four of the beams analyzed in the preceding section for derivation of the tensile stress block. With reference to the values of stress block parameters in Table 1 for beams under two-point load configuration, the values of stress block parameters α_1, α_{2i} and α_2 are taken as 0.5, 16 and 50, respectively. Using the tensile stress block with such parametric values, member analysis is carried out to determine the moment-deflection response of the beams. As shown in Figs. 13 and 14, the member analysis results are in excellent agreement with the experimental results. Furthermore, the two beams are analyzed by means of finite element method using the same materials constitutive models and procedures presented in Section 3 of this paper, and the computed moment-deflection response is also plotted in Figs. 13 and 14. It can be seen that the finite element analysis results are in excellent agreement with the experimental results as well. In comparison with the finite element method, member analysis is less complicated to implement, yet it can yield similarly high accuracy.

6.2. *Beams CB2B-1 and CB3B-1 tested by Masmoudi et al. [56]*

Beam specimens CB2B-1 and CB3B-1 tested by Masmoudi et al. [56] are selected for analysis. Fig. 15 depicts the layout of the beams. The geometric and material characteristics of the beams are listed in the fourth and last columns of Table 2. The beams had length of 3300 mm and span of 3000 mm. They were subjected to symmetrical two-point loads with shear span of 1250 mm. The beams had uniform cross-section of 200 × 300 mm (breadth b × depth h). Beam CB2B-1 was reinforced with two 14.9 mm diameter FRP tension reinforcement and two 10 mm diameter steel compression reinforcement. Beam CB3B-1 was reinforced with three 14.9 mm diameter FRP tension reinforcement and two 10 mm diameter steel compression reinforcement. The FRP bars had ultimate tensile strength and modulus of elasticity of 773 MPa and 38 GPa, respectively. For both beams, steel stirrups of 10 mm diameter at 80 mm spacing were provided throughout the length of beam except the region of 200 mm at both sides from the mid-span. The

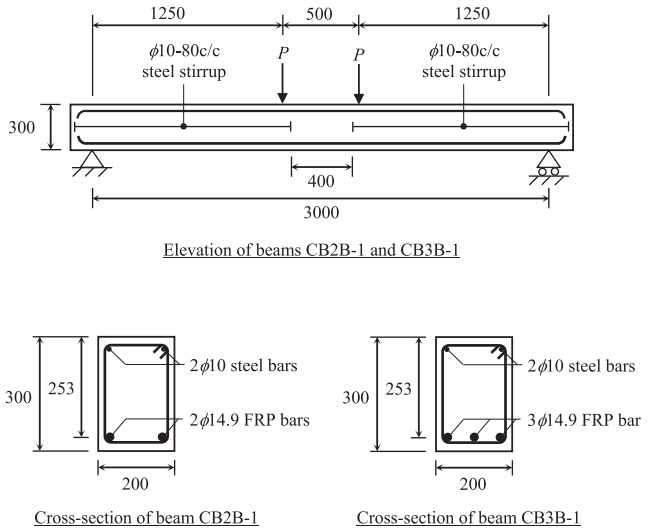

Fig. 15. Layout of beams CB2B-1 and CB3B-1 (dimensions in mm).

steel compression reinforcement and stirrups had yield strength of 480 MPa, ultimate strength of 600 MPa, and modulus of elasticity of 200 GPa. For concrete, the compressive strength and modulus of elasticity were respectively 52 MPa and 33 GPa.

Figs. 16 and 17 present the experimental and analytical moment versus mid-span deflection curves of beam specimens CB2B-1 and CB3B-1. According to the reported results by Masmoudi et al. [56], both specimens were failed by crushing of concrete. Similar to the observation from beams ISO1 and ISO3, the ACI-440 equation of effective moment of inertia predicts higher post-crack flexural stiffness than the experimental results, and hence underestimates the deflection. The discrepancy is more apparent for beam specimen CB2B-1 with lower ρ_{ft}. Thus, the ACI-440 equation tends to overestimate the post-crack flexural stiffness of FRP-RC beams, especially for beams with lower FRP tension reinforcement ratio. It should be borne in mind that such overestimation is not on the conservative side. Nevertheless, the accuracy could be improved by suitable adjustment of the relevant empirical coefficient.

Though both beams CB2B-1 and CB3B-1 are subjected to two-point load, the distance between load application points is approximately 16.7% rather than one-third of the span length, and therefore the load configuration is not the same as the beams analyzed in the preceding section for derivation of the tensile stress block. Nonetheless, it would be highly desirable from practical design viewpoint if the same set of parametric values can be used for different load configurations that are frequently encountered. To explore the feasibility of adhering to use a

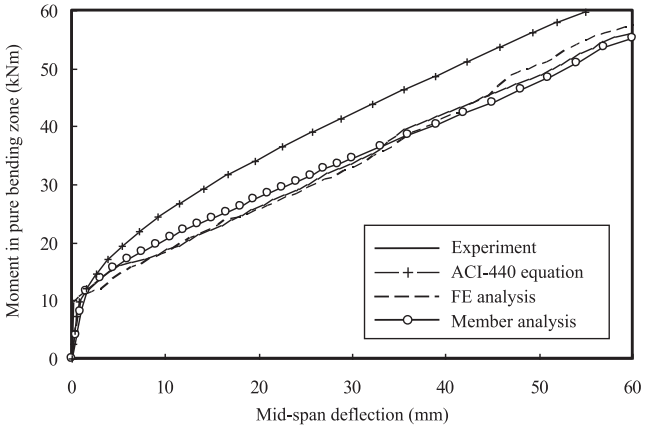

Fig. 16. Moment-deflection curves of beam CB2B-1.

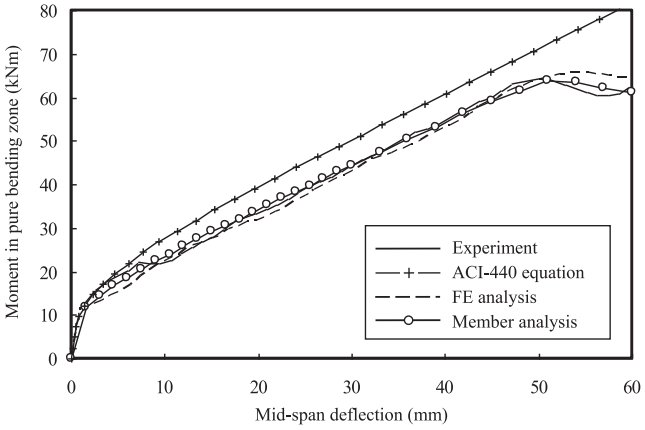

Fig. 17. Moment-deflection curves of beam CB3B-1.

representative set of parametric values, with reference to the computation for beams ISO1 and ISO3, the values of stress block parameters α_1, α_{2i} and α_2 are taken as 0.5, 16 and 50, respectively, for conducting member analysis of beams CB2B-1 and CB3B-1. The resulting moment-deflection curves as shown in Figs. 16 and 17 again demonstrate excellent agreement with the experimental response, when the same set of parametric values is used. Furthermore, the two beams are analyzed by means of finite element method in the same manner as for beams ISO1 and ISO3, and the computed moment-deflection response is also plotted in Figs. 16 and 17. Once again it is seen that the finite element analysis results are in excellent agreement with the experimental results. Overall, the use of member analysis method in combination with the tensile stress block is accurate and simple to implement, and is recommended for deformation analysis of FRP-RC beams. Further analysis and valuation of stress block parameters for FRP-RC beams of a wider range of structural configurations are recommended for future research, in order to refine and extend the applicability of the proposed tensile stress block.

7. Conclusions

Fibre-reinforced polymer (FRP) offers discernible advantages over conventional steel reinforcement that justify its usage as alternative reinforcement material in concrete structures. This study has addressed the deformation analysis of FRP reinforced concrete (FRP-RC) beams. Tension-stiffening of cracked FRP-RC beams has been considered via the use of semi-empirical equations to compute effective flexural stiffness, nonlinear finite element analysis, and the use of tensile stress block in conjunction with member analysis. In structural engineering practice, member analysis in combination with tensile stress block is an effective means for serviceability assessment that can circumvent the use of sophisticated theoretical models and constitutive laws. Based on the tension stress fields obtained from nonlinear finite element analysis for a series of FRP-RC beams, parametrized tensile stress block for deformation analysis of FRP-RC beams has been derived, and mathematical equations defining the stress block have been proposed. The stress block consists of a linear ascending branch and a bilinear descending branch, which respectively represent the behaviour of uncracked and cracked flexural tensile reinforced concrete elements. The geometry of the stress block is defined by three parameters, whose values have been determined for various FRP tension reinforcement ratios and types of load.

Experimental FRP-RC beam specimens tested in the literature have been analyzed by means of the effective moment of inertia as per the codified equation in ACI (American Concrete Institute) Committee 440, by means of nonlinear finite element method, and by means of the proposed tensile stress block in combination with member analysis. From the results of moment-deflection response, it has been found that

the ACI codified equation of effective moment of inertia generally underestimates the deflection of cracked FRP-RC beams, and is non-conservative from the serviceability assessment viewpoint. On the other hand, excellent agreement between the experimental results, member analysis results and finite element analysis results has been achieved, thereby endorsing the applicability and reliability of the proposed tensile stress block for FRP-RC beams. The authors advocate the use of member analysis in combination with the tensile stress block for prediction of deformational behaviour of FRP-RC beams.

Acknowledgements

This project has received funding from European Social Fund (Project No. 09.3.3-LMT-K-712-01-0145) under a grant agreement with the Research Council of Lithuania (LMTLT).

References

[1] Abrishambaf A, Barros JAO, Cunha VMCF. Tensile stress–crack width law for steel fibre reinforced self-compacting concrete obtained from indirect (splitting) tensile tests. Cem Concr Compos 2015;57:153–65.
[2] ACI Committee 318. Building Code Requirements for Structural Concrete and Commentary, ACI 318M-14. Michigan, USA: American Concrete Institute; 2014. p. 473.
[3] ACI Committee 440. Guide for the Design and Construction of Structural Concrete Reinforced with FRP Bars, ACI 440.1R-15. Michigan, USA: American Concrete Institute; 2015. p. 44.
[4] Achillides Z. Bond Behaviour of FRP Bars in Concrete (PhD Thesis). Sheffield, UK: University of Sheffield; 1998. p. 355 pp..
[5] Al-Sunna R, Pilakoutas K, Waldron P, Al-Hadeed T. Deflection of FRP reinforced concrete beams. Proceedings, Fourth Middle East Symposium on Structural Composites for Infrastructure Applications, Alexandria, Egypt. 2005.
[6] Baena M, Torres Ll, Turon A, Barris C. Experimental study of bond behaviour between concrete and FRP bars using a pull-out test. Compos B Eng 2009;40(6):784–97.
[7] Baena M, Torres Ll, Turon A, Miàs C. Analysis of cracking behavior and tension stiffening in FRP reinforced concrete tensile elements. Compos B 2013;45(1):1360–7.
[8] Bangash MYH. Manual of Numerical Methods in Concrete: Modelling and Applications Validated by Experimental and Site-Monitoring Data. London, U.K.: Thomas Telford; 2001. p. 918.
[9] Barros JAO. Behavior of Fibre Reinforced Concrete. Experimental Analysis and Numerical Simulation (in Portuguese) (PhD. Thesis). Portugal: Faculty of Engineering, University of Porto; 1995.
[10] Beeby AW, Scott RH, Jones AEK. Revised code provisions for long-term deflection calculations. Proc Inst Civil Eng, Struct Build 2005;158(1):71–5.
[11] Benmokrane B, Chaallal O, Masmoudi R. Flexural response of concrete beams reinforced with FRP reinforcing bars. ACI Struct J 1996;93(1):730–42.
[12] Bischoff PH, Paixao R. Tension stiffening and cracking of concrete reinforced with glass fiber reinforced polymer (GFRP) bars. Can J Civ Eng 2004;31(4):579–88.
[13] Bischoff PH. Deflection calculation of FRP reinforced concrete beams based on modifications to the existing Branson equation. J Compos Construct, ASCE 2007;11(1):4–14.
[14] Bischoff PH, Scanlon A. Effective moment of inertia for calculating deflections of concrete members containing steel reinforcement and fiber-reinforced polymer reinforcement. ACI Struct J 2007;104(1):68–75.
[15] Bischoff PH, Gross SP. Design approach for calculating deflection of FRP-reinforced concrete. J Compos Construct, ASCE 2011;15(4):490–9.
[16] Branson DE. Design procedures for computing deflection. ACI J 1968;65(9):730–42.
[17] Branson DE. Deformation of concrete structures. New York: McGraw-Hill; 1977. p. 546.
[18] Cairns JW, Metelli G, Plizzari GA. Proceedings, 4th International Conference Bond in Concrete: Bond in New Materials and under Severe Conditions, Brescia, Italy, (2012).
[19] Carpinteri A. Applications of fracture mechanics to reinforced concrete. Oxon: Taylor & Francis; 2005. p. 616.
[20] Carreira DJ, Chu K. The moment-curvature relationship of reinforced concrete members. ACI J 1986;83(2):191–8.
[21] Castel A, Vidal T, François R. Effective tension active cross-section of reinforced concrete beams after cracking. Mater Struct 2006;39(1):115–26.
[22] Cosenza E, Manfredi G, Realfonzo R. Behavior and modeling of bond of FRP rebars to concrete. J Compos Construct, ASCE 1997;1(2):40–51.
[23] Dabbagh H, Foster SJ. A smeared-fixed crack model for FE analysis of RC membranes incorporating aggregate interlock. Adv Struct Eng 2006;9(1):91–102.
[24] Darwin D, Pecknold DA. Nonlinear biaxial stress-strain law for concrete. J Eng Mech Divi, ASCE 1977;103(2):229–41.
[25] Eligehausen R, Popov EP, Bertero VV. Local Bond Stress-Slip Relationships of Deformed Bars under General Excitations: Experimental Results and Analytical Model Report No UCB/EERC-83/23 Berkeley, USA: Earthquake Research Center, University of California; 1983. p. 169.
[26] Fava G, Carvelli V, Pisani MA. Remarks on bond of GFRP rebars and concrete. Compos B Eng 2016;93:210–20.
[27] fib (Fédération international du béton) (2000), Bond of Reinforcement in Concrete, fib Bulletin 10, Lausanne, Switzerland.
[28] fib (Fédération international du béton) (2007), FRP Reinforcement in RC Structures, fib Bulletin 40, Lausanne, Switzerland.
[29] fib (Fédération international du béton) (2008), Constitutive Modelling of High Strength/High Performance Concrete, fib Bulletin 42, Lausanne, Switzerland.
[30] Focacci F, Nanni A, Bakis CE. Local bond-slip relationship for FRP reinforcement in concrete. J Compos Construct, ASCE 2000;4(1):24–31.
[31] Frantzeskakis C, Theillout JN. Nonlinear finite element analysis of reinforced concrete structures with a particular strategy following the cracking process. Comput Struct 1989;31(3):395–412.
[32] Gao D, Benmokrane B, Masmoudi R. A Calculating Method of Flexural Properties of FRP-reinforced Concrete Beam. Part 1: Crack Width and Deflection Technical Report Sherbrooke, Quebec, Canada: Department of Civil Engineering, University of Sherbrooke; 1998 p. 24.
[33] Gilbert RI, Warner RF. Tension stiffening in reinforced concrete slabs. J Struct Eng Divi, ASCE 1978;104(12):1885–900.
[34] Goodman RE, Taylor RL, Brekke TL. A model for the mechanics of jointed rock. J Soil Mech Found Divi, ASCE 1968;94(3):637–59.
[35] Gudonis E, Timinskas E, Gribniak V, Kaklauskas G, Arnautov AK, Tamulenas V. FRP reinforcement for concrete structures: state-of-the-art review of application and design. Eng Struct Technol 2013;5(4):147–58.
[36] Guo ZH, Zhang XQ. Investigation of complete stress-deformation curves of concrete in tension. ACI Mater J 1987;84(4):278–85.
[37] Hammoud R, Boukhili R, Yahia A. Unified formulation for a triaxial elastoplastic constitutive law for concrete. Materials 2013;6(9):4226–48.
[38] He XG, Kwan AKH. Modeling dowel action of reinforcement bars for finite element analysis of concrete structures. Comput Struct 2001;79(6):595–604.
[39] Jakubovskis R, Kaklauskas G, Gribniak V, Weber A, Juknys M. Serviceability analysis of concrete beams with different arrangements of GFRP bars in the tensile zone. J Compos Construct, ASCE 2014;18(5):04014005.
[40] Kaklauskas G, Ghaboussi J. Stress-strain relations for cracked tensile concrete from RC beam tests. J Struct Eng, ASCE 2001;127(1):64–73.
[41] Khan QS, Sheikh MN, Hadi MNS. Tension and compression testing of fibre reinforced polymer (FRP) bars. Proceedings, The 12th International Symposium on Fiber Reinforced Polymers for Reinforced Concrete Structures & The 5th Asia-Pacific Conference on Fiber Reinforced Polymers in Structures, Nanjing, China. 2015.
[42] Kocaoz S, Samaranayake VA, Nanni A. Tensile characterization of glass FRP bars. Compos B Eng 2005;36(2):127–34.
[43] Kupfer HB, Gerstle KH. Behaviour of concrete under biaxial stresses. J Eng Mech Divi, ASCE 1973;99(4):853–66.
[44] Kwak HG, Kim SP. Monotonic moment-curvature relation of an RC beam. Mag Concr Res 2002;54(6):423–34.
[45] Kwak HG, Kim JK. Implementation of bond-slip effect in analyses of RC frames under cyclic loads using layered section method. Eng Struct 2006;28(12):1715–27.
[46] Kwan AKH, Lam JYK, Ng PL. Tension stiffening in reinforced concrete beams: A new tensile stress block. In: Choi CK, editor. The Proceedings of 4th International Conference on Advances in Structural Engineering and Mechanics, Jeju, Korea. 2008. p. 2357–68.
[47] Kwan AKH, Ng PL, Lam JYK. Modelling dowel action of discrete reinforcing bars in cracked concrete structures. In: Lu JWZ, Leung AYT, Iu VP, Mok KM, editors. Proceedings of the Second International Symposium on Computational Mechanics and the Twelfth International Conference on the Enhancement and Promotion of Computational Methods in Engineering and Science, Hong Kong. 2009. p. 701–6.
[48] Kwan AKH, Leung AYT, Ng PL. Adaptive constrained mesh generation: part 2 – accommodation of constraints. Int J Appl Math Mech 2010;6(8):22–45.
[49] Kwan AKH, Ng PL. Modelling dowel action of discrete reinforcing bars for finite element analysis of concrete structures. Comput Concr 2013;12(1):19–36.
[50] Lam JYK, Ng PL, Kwan AKH. Nonlinear multilevel analysis of reinforced concrete beams. In: Topping BHV, editor. Proceedings of the Eleventh International Conference on Civil, Structural and Environmental Engineering Computing, St. Julians, Malta. 2007. p. 16.
[51] Lam JYK, Ng PL, Kwan AKH. Tension stiffening in reinforced concrete beams: part 2 – section and member analysis. Proc Inst Civil Eng, Struct Build 2010;163(1):29–39.
[52] Lee SC, Cho JY, Vecchio FJ. Model for post-yield tension stiffening and rebar rupture in concrete members. Eng Struct 2011;33(5):1723–33.
[53] Lin XS, Zhang YX. Evaluation of bond stress-slip models for FRP reinforcing bars in concrete. Compos Struct 2014;107:131–41.
[54] Ma FJ, Ng PL, Kwan AKH. “Finite element analysis of RC tension member based on pseudo-discrete crack model”. In: Choi CK, editor. The 2017 World Congress on Advances in Structural Engineering and Mechanics, Ilsan (Seoul), Korea. 2017. p. 13.
[55] Marti P, Alvarez M, Kaufmann W, Sigrist V. Tension chord model for structural concrete. Struct Eng Int 1998;8(4):287–98.
[56] Masmoudi R, Theriault M, Benmokrane B. Flexural behavior of concrete beams reinforced with deformed fibre reinforced plastic reinforcing rods. ACI Struct J 1998;95(6):668–76.
[57] Mazaheripour H, Barros JAO, Pepe M, Giliberti A, Martinelli E. Experimental and theoretical study on bond behavior of GFRP bars in steel fiber reinforced self compacting concrete. 4th International Symposium – Bond in Concrete: Bond, Anchorage, Detailing, Brescia, Italy. 2012.
[58] Mazaheripour H, Barros JAO, Soltanzadeh F, Gonçalves D. Interfacial bond behaviour of GFRP bar in self-compacting fiber reinforced concrete. In: Barros JAO,

editor. Proceedings, 8th RILEM International Symposium on Fibre Reinforced Concrete: Challenges and Opportunities, Guimarães, Portugal. 2012. p. 13.
[59] Mazaheripour H, Barros JAO, Sena-Cruz JM, Pepe M, Martinelli E. Experimental study on bond performance of GFRP bars in self-compacting steel fibre reinforced concrete. Compos Struct 2013;95:202–12.
[60] Mazaheripour H, Barros JAO, Sena-Cruz JM. Tension-stiffening model for FRC reinforced by hybrid FRP and steel bars. Compos B 2016;88:162–81.
[61] Mousavi SR, Esfahani MR. Effective moment of inertia prediction of FRP-reinforced concrete beams based on experimental results. J Compos Construct, ASCE 2012;16(5):490–8.
[62] Murray A, Gilbert RI, Castel A. Study of disturbed strain regions for serviceability analysis of cracked RC flexural members. In: Hong H, Zhang C, editors. 24th Australasian Conference on the Mechanics of Structures and Materials, Perth, Australia. 2017. p. 97–102.
[63] Nayal R, Rasheed HA. Tension stiffening model for concrete beams reinforced with steel and FRP bars. J Mater Civ Eng ASCE 2006;18(6):831–41.
[64] Ng PL, Lam JYK, Kwan AKH. Tension stiffening in reinforced concrete beams: part 1 – finite element analysis. Proc Inst Civil Eng, Struct Build 2010;163(1):19–28.
[65] Ng PL, Kwan AKH, Leung AYT. Adaptive constrained mesh generation: part 1 – stripwise advancing front technique. Int J Appl Math Mech 2010;6(8):1–21.
[66] Ng PL, Lam JYK, Kwan AKH. Effects of concrete-to-reinforcement bond and loading conditions on tension stiffening. Procedia Eng 2011;14:704–14.
[67] Ng PL, Kwan AKH, Lam JYK. Tension stiffening in concrete beams subjected to small axial load. In: Seoul Korea, Choi CK, editors. Proceedings of the 2011 World Congress on Advances in Structural Engineering and Mechanics. 2011. p. 1605–20.
[68] Ng PL, Ma FJ, Kwan AKH. Fernando D, Teng JG, Torero JL, editors. Crack analysis of concrete beams based on pseudo-discrete crack modelProceedings of the Second International Conference on Performance-based and Life-cycle Structural Engineering, Brisbane, Australia. 2015. p. 669–78.
[69] Ng PL, Lam JYK, Kwan AKH. Nonlinear multilevel analysis of reinforced concrete frames. J Eng Struct Technol 2015;7(4):168–76.
[70] Ng PL, Gribniak V, Jakubovskis R, Rimkus A. Tension stiffening approach for deformation assessment of flexural reinforced concrete members under compressive axial load. Struct Concr 2019;20:1–13. https://doi.org/10.1002/suco.201800286.
[71] Noh SY. Tension stiffening model for numerical analysis of RC structure by using bond-slip relationship. J Adv Concr Technol 2009;7(1):61–78.
[72] Pepe M, Mazaheripour H, Barros JAO, Sena-Cruz J, Martinelli E. Numerical calibration of bond law for GFRP bars embedded in steel fibre-reinforced self-compacting concrete. Compos B 2013;50:403–12.
[73] Saenz LP. Discussion of 'Equation for the stress-strain curve of concrete' by Desayi and Krishnan. ACI J 1964;61(9):1229–35.
[74] Schnobrich WC. Role of finite element analysis of reinforced concrete structures. In: Meyer C, Okamura H, editors. Proceedings, Seminar on Finite Element Analysis of Reinforced Concrete Structures, Tokyo, Japan. 1985. p. 1–24.
[75] Salem H, Maekawa K. Spatially averaged tensile mechanics for cracked concrete and reinforcement under highly inelastic range. J Mater, Concr Struct Pavements, JSCE 1999;613(42):277–93.
[76] Sena-Cruz A, Barros JAO, Azevedo Á. Elasto-plastic Multi-fixed Smeared Crack Model for Concrete Report 04-DEC/E-05 Portugal: University of Minho; 2006 p. 70.
[77] Sooriyaarachchi H, Pilakoutas K, Byars E. Tension stiffening behavior of GFRP-reinforced concrete. ACI Special Publication SP-230, 7th International Symposium on Fiber Reinforced Polymer Reinforcement for Reinforced Concrete Structures (FRPRCS-7), New Orleans, Louisiana, USA. 2005. p. 975–90.
[78] Theriault M, Benmokrane B. Effects of FRP reinforcement ratio and concrete strength on flexural behavior of concrete beams. J Compos Constr 1998;2(1):7–16.
[79] Torres Ll, Lopez-Almansa F, Bozzo LM. Tension-stiffening model for cracked flexural concrete members. J Struct Eng, ASCE 2004;130(8):1242–51.
[80] Walraven JC. Aggregate Interlock: A Theoretical and Experimental Analysis (PhD. Thesis). The Netherlands: Delft University of Technology; 1980. p. 197.
[81] Yan F, Lin ZB, Yang MJ. Bond mechanism and bond strength of GFRP bars to concrete: a review. Compos B Eng 2016;98:56–69.
[82] Yost JR, Gross SP, Dinehart DW. Effective moment of inertia for glass fiber-reinforced polymer-reinforced concrete beams. ACI Struct J 2003;100(6):732–9.
[83] Zaman A, Gutub SA, Wafa MA. A review on FRP composites applications and durability concerns in the construction sector. J Reinf Plast Compos 2013;32(24):1966–88.
[84] Zhu BF. The Finite Element Method: Fundamentals and Applications in Civil, Hydraulic, Mechanical and Aeronautical Engineering. Singapore: Wiley; 2018. p. 843.